Tetrahedron: *Asymmetry* 22 (2011) 283–293

Contents lists available at ScienceDirect

Tetrahedron: *Asymmetry*

journal homepage: www.elsevier.com/locate/tetasy

Looking glass mechanism-based inhibition of peptidylglycine α-amidating monooxygenase

Michael S. Foster, Charlie D. Oldham, Sheldon W. May *

School of Chemistry and Biochemistry and the Petit Institute for Bioengineering and Biosciences, Georgia Institute of Technology, Atlanta, GA 30332, USA

ARTICLE INFO

Article history:
Received 14 December 2010
Accepted 12 January 2011
Available online 4 March 2011

ABSTRACT

Carboxyl-terminal amidation, a required post-translational modification for the bioactivation of many peptide hormones, entails sequential enzymatic action by peptidylglycine α-monooxygenase (PAM, EC 1.14.17.3) and peptidylamidoglycolate lyase (PGL, EC 4.3.2.5). We have previously demonstrated that PAM and PGL exhibit strict tandem reaction stereospecificities, with PAM producing exclusively α-hydroxyglycine moieties of absolute configuration (*S*), and PGL being reactive only toward (*S*)-α-hydroxyglycines, and we have also shown that PAM exhibits strict P_2-subsite stereospecificity toward both peptide substrates and peptidyl competitive inhibitors. Herein, it is reported that the inhibitory stereochemistry of olefinic mechanism-based amidation inhibitors differs from the strict subsite stereospecificity exhibited by PAM toward substrates and reversible competitive inhibitors. Kinetic analyses of mechanism-based irreversible inhibition of PAM by the (*S*)- and (*R*)-enantiomers of 5-acetamido-4-oxo-6-phenyl-2-hexenoic acid were carried out using the rigorous progress curve method. The two enantiomers were found to exhibit very similar values of K_I and k_{inact} and in both cases kinetic analysis confirmed that irreversible inhibition occurs strictly at the substrate binding site with no ESI complex being formed during the catalytic processing of these irreversible inhibitors. Molecular docking studies were carried out to help rationalize the sharp contrast in the stereospecificity of PAM toward irreversible inhibitors versus substrates and competitive inhibitors. The results revealed that, in contrast to substrates, both docked enantiomers of the olefinic irreversible inhibitors are well-positioned to undergo catalytic processing at the Cu center that gives rise to irreversible inhibition. Taken together, these results provide one of the first clear examples where the stereospecificity of a particular enzyme toward mechanism-based irreversible inhibitors differs from that for substrates and competitive inhibitors.

1. Introduction

Carboxyl-terminal amidation is a common post-translational event responsible for the bioactivation of approximately half of all peptide hormones, including the potent pro-inflammatory mediators Substance P and Calcitonin Gene-Related Peptide (CGRP)[1–3] often increasing the affinity for their respective receptors by as much as 1000-fold compared to their glycine-extended precursors.[4] The amidation reaction is catalyzed by the sequential activities of peptidylglycine α-monooxygenase [PAM; EC 1.14.17.3] and peptidoamidoglycolate lyase [EC 4.3.2.5] upon precursor C-terminal glycine-extended peptide substrates.[5–16] In a process that is dependent on ascorbate and molecular oxygen, PAM stereospecifically catalyzes the formation of an (*S*)-α-hydroxyglycine intermediate from glycine-extended peptides with amino acid residues of L-configuration at the P_2-position. Correspondingly, we have shown that PGL, which converts the intermediate to the des-glycyl amide plus glyoxylate, is reactive only toward α-hydroxyglycines with an (*S*)-absolute configuration.[9,16] We have also shown that the glycolate ester analogs of glycine-extended peptides are potent competitive inhibitors of PAM, but only when an L-amino acid residue is present at the P_2-subsite position.[16] Thus, PAM exhibits subsite stereospecificity toward both peptide substrates and peptidyl competitive inhibitors.

Recognizing the potential pharmacological benefit of inhibiting the synthesis of pro-inflammatory peptides, we have developed new classes of mechanism-based irreversible inhibitors and transition-state analogs targeted at the post-translational amidation process. Among these, compounds 5-acetamido-4-oxo-6-phenyl-2-hexenoic acid (AOPHA) and 5-acetamido-4-oxo-6-thienyl-2-hexenoic acid, which possess a C-terminal acrylate functionality linked to a PAM-binding peptide moiety, are the most potent irreversible amidation inhibitors known to date.[17,6,18,19] Indeed, we have recently shown that irreversible PAM inhibitors exhibit potent anti-inflammatory activity against both acute (carrageenan) and chronic (adjuvant-induced polyarthritis) inflammation in

* Corresponding author. Tel.: +1 404 894 4052; fax: +1 404 894 2295.
E-mail address: sheldon.may@chemistry.gatech.edu (S.W. May).

0957-4166/$ - see front matter © 2011 Elsevier Ltd. All rights reserved.
doi:10.1016/j.tetasy.2011.01.006

rats.[20,21] We have also shown that the methyl ester of 4-phenyl-3-butenoic acid (PBA-OMe), an irreversible PAM inhibitor, is able to restore gap-junctional communication in WB-Ras-transformed rat liver epithelial cells, and is selectively cytotoxic toward transformed cells versus untransformed WB-Neo cells.[22]

Stereospecificity is obviously a very important consideration in the design of enzyme-targeted pseudosubstrates, reversible inhibitors, and irreversible inhibitors. As pointed out by Kim, while binding stereospecificities for competitive inhibitors and transition-state analogs would generally be expected to correspond to those for substrates, evidence has begun to emerge that the inhibitory stereochemistry for mechanism-based irreversible inhibitors may be quite different from that predicted on the basis of substrate reactivity.[23–25] Herein, we report that the inhibitory stereochemistry of olefinic mechanism-based irreversible amidation inhibitors indeed differs from the strict subsite stereospecificity exhibited by PAM toward both substrates and competitive inhibitors.

2. Results

2.1. Kinetic analyses of PAM inhibition by (*S*)- and (*R*)-5-acetamido-4-oxo-6-phenyl-2-hexenoic acid

In order to ensure the enantiomeric purity of the tested compounds, each synthesis began with the appropriate enantiomerically pure amino acid methyl ester. Prior to the final hydrolysis step, each enantiomer of AOPHA-Me was eluted from a chiral D-penicillamine column as a single peak (21 and 28 min for the D and L-enantiomers, respectively) using the procedure outlined in Section 4. Both enantiomers had identical profiles by ESI mass spectrometry and NMR. Each enantiomeric ester was then enzymatically hydrolyzed to the free acid using porcine liver esterase (E.C. 3.1.1.1). This enzyme was employed to allow for more mild alkaline conditions than would be utilized in a base-catalyzed hydrolysis. Each enantiomer of AOPHA showed only one peak upon eluting from the D-penicillamine column, and two peaks when run together as a mixture. The enantiomeric purity was further investigated using polarimetry and circular dichroism spectroscopy. The Cotton effect was clearly evident at 205 nm for the enantiomeric pair. Polarimetry indicated that the (*R*)- and (*S*)-enantiomers rotate polarized light by the same magnitude but in opposite directions, with specific $[\alpha]_D$ values of +12 and −12 for (*R*)-AOPHA and (*S*)-AOPHA, respectively. ESI mass spectrometry and NMR again showed that both compounds had identical profiles. These results clearly indicate that enantiomeric purity was maintained throughout these syntheses.

Kinetic analyses of the irreversible inhibition of PAM by the (*S*)- and (*R*)-enantiomers of AOPHA were carried out using both the conventional 'dilution assay' method and the much more rigorous 'progress curve' method.[17,26,27] Whereas the dilution assay is quite straightforward, it reliably provides only the value of k_{inact}/K_I and not the individual constants. On the other hand, the progress curve method, owing to the simultaneous incubation of both substrate and inhibitor, allows for the elucidation of all possible kinetic constants and is therefore able to clearly indicate the type of inhibition which occurs. As detailed by Tsou,[28] progress curves of inhibition are obtained at a series of substrate and inhibitor concentrations; then, through a series of replots, numerical values are obtained for each of the kinetic parameters shown in the scheme in Table 1. This scheme illustrates the nature of all possible pathways when the enzyme is incubated simultaneously in the presence of both substrate and inhibitor.

Representative progress curves and double reciprocal plots for both enantiomers of AOPHA are shown in Figure 1, and the kinetic parameters obtained from these experiments are listed in Table 1. It is evident that the K_I values for each enantiomer are remarkably similar, with values of 53.7 and 60.0 μM obtained from the progress curve assay for the (*S*)- and (*R*)-enantiomers, respectively. The rate constants for irreversible inhibition are also very similar: 0.38 and 0.29 min^{-1} for the (*S*)- and (*R*)-enantiomers, respectively. Double-reciprocal plots for both enantiomers (Fig. 1c and d) show a convergence of all lines (each representative of a different

Table 1
Inhibition scheme and kinetic parameters for PAM inhibition by olefins

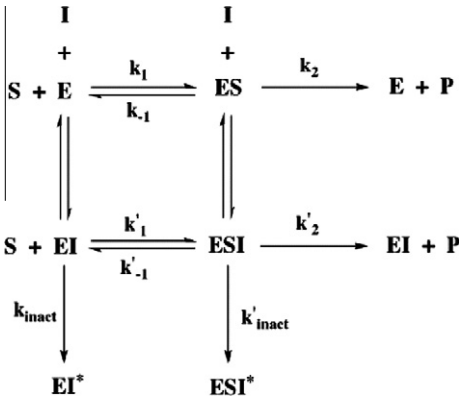

	(*S*)-5-Acetamido-4-oxo-6-phenyl-2-hexenoic acid	(*R*)-5-Acetamido-4-oxo-6-phenyl-2-hexenoic acid	(*S*)-5-Acetamido-7-methylthio-4-oxo-2-heptenoic acid
K_I (μM)	54 ± 1	60 ± 2	57 ± 1
K'_I (MM)	∞	∞	∞
k_{inact} (min^{-1})	0.38 ± 0.04	0.29 ± 0.02	0.14 ± 0.01
k'_{inact} (min^{-1})	0	0	0
k'_2 (min^{-1})	0	0	0
k_{inact}/K_I (M^{-1} min^{-1} × 10^{-3})	7.0 ± 0.2	4.8 ± 0.1	2.4 ± 0.1
k_{inact}/K_I (M^{-1} min^{-1} × 10^{-3}) (dilution assay)	7.3 ± 0.1	4.1 ± 0.1	ND
K_M (methyl ester, PLE)	8.6 mM	6.1 mM	ND
V_{max} (methyl ester, PLE)	0.058 mM s^{-1}	0.048 mM s^{-1}	ND

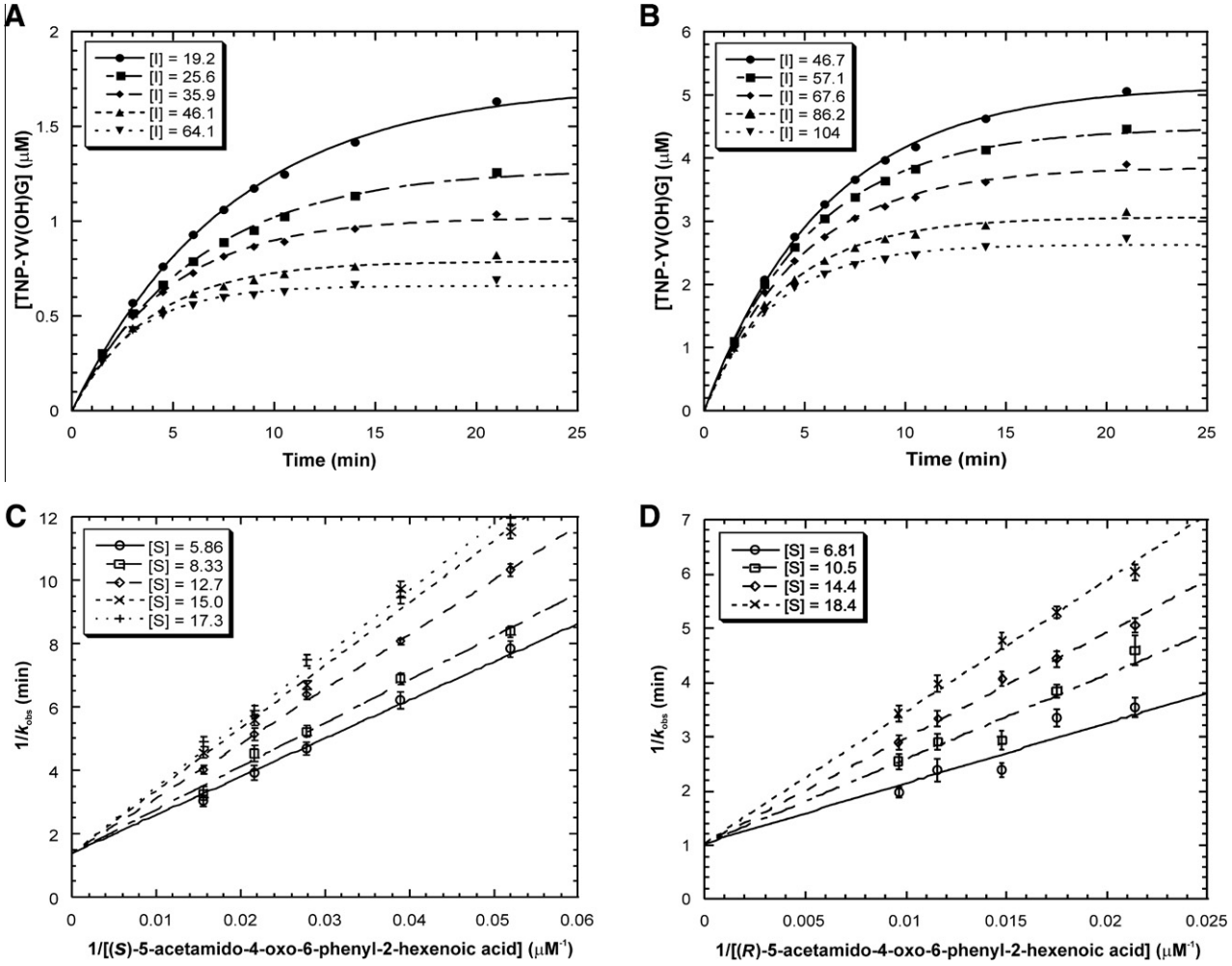

Figure 1. Progress curves and double-reciprocal plots for PAM inhibition by AOPHA enantiomers. Product formation in the presence of various concentrations of (*S*)-5-acetamido-4-oxo-6-phenyl-2-hexenoic acid and (*R*)-5-acetamido-4-oxo-6-phenyl-2-hexenoic acid. (A) Inhibition by (*S*)-5-acetamido-4-oxo-6-phenyl-2-hexenoic acid between 19.2 and 64.1 μM at a substrate (TNP-YVG) concentration of 5.86 μM. (B) Inhibition by (*R*)-5-acetamido-4-oxo-6-phenyl-2-hexenoic acid between 46.7 and 104 μM at a substrate concentration of 18.4 μM. Asymptotes represent the product concentration at time = infinity. Subsequent replots yield the kinetic parameters listed in Table 1. (C) Double-reciprocal plot of 1/kobs versus 1/[*I*] for (*S*)-5-acetamido-4-oxo-6-phenyl-2-hexenoic acid. (D) Double-reciprocal plot of 1/kobs versus 1/[*I*] for (*R*)-5-acetamido-4-oxo-6-phenyl-2-hexenoic acid.

substrate concentration) at the same point on the *y*-axis, as expected for inhibition that occurs only at the substrate binding site.[28,17] In addition, k'_{inact} was found to be zero for both enantiomers, indicating that no inactivated ESI complex is formed from ESI; the fact that k'_2 is zero for each compound also shows that no product is formed and released from the ESI complex. Moreover, the inhibition constant K'_I was found to approach infinity for both enantiomers, indicating that a ternary complex never forms in any case, and is consistent with the zero values for k'_2 and k'_{inact}. Taken together, these results clearly demonstrate that inhibition of PAM by both (*R*)- and (*S*)-AOPHA occurs strictly at the PAM substrate binding site, with no 'ESI' complex being formed during catalytic processing of these irreversible inhibitors.

In view of this near equipotency of the two AOPHA enantiomers as irreversible inhibitors of PAM, we also investigated the relative reactivities of the two enantiomers of AOPHA-Me as substrates of Porcine Liver Esterase (PLE). Michaelis–Menten plots and Hanes–Woolf replots for (*S*)-AOPHA-Me and (*R*)-AOPHA-Me are shown in Figure 2. The K_M values for the (*S*)- and (*R*)-enantiomers are 8.6 and 6.1 mM, respectively, and the respective V_{max} values at identical concentrations of enzyme are 0.06 and 0.05 mM s^{-1}. PLE has been shown, in many different cases, to be stereoselective, but generally research has been limited to molecules which possess stereocenters either immediately adjacent to, or within two atoms of, the oxygen atom of the ester moiety.[29]

2.2. Molecular docking of substrate enantiomers

We carried out a series of protein–ligand molecular docking studies in an attempt to rationalize the sharp contrast in the stereospecificity of PAM toward the mechanism-based irreversible AOPHA inhibitors on the one hand, versus peptide substrates and glycolate-ester competitive inhibitors on the other. Obviously, a key structural difference between these three classes of compounds is the nature of the atom present at the position analogous to that of the amide nitrogen (hydrogen bond donor) of the C-terminal-Gly in PAM substrates, such as *N*-Ac-Phe-Gly; the competitive inhibitors possess an ester oxygen atom in this position (hydrogen bond acceptor), and the olefinic irreversible inhibitors possess an sp^2-hybridized carbon atom (neither a hydrogen bond donor nor acceptor).

The structures of AOPHA and many of our competitive inhibitors were designed on the basis of the active PAM substrate, *N*-Ac-L-Phe-Gly (K_M = 7.9 μM).[16] On the other hand, the crystal structure determined by Amzel et al. was for the PAM catalytic core complexed with the ligand *N*-Ac-3,5-diiodo-L-Tyr-Gly.[30] In

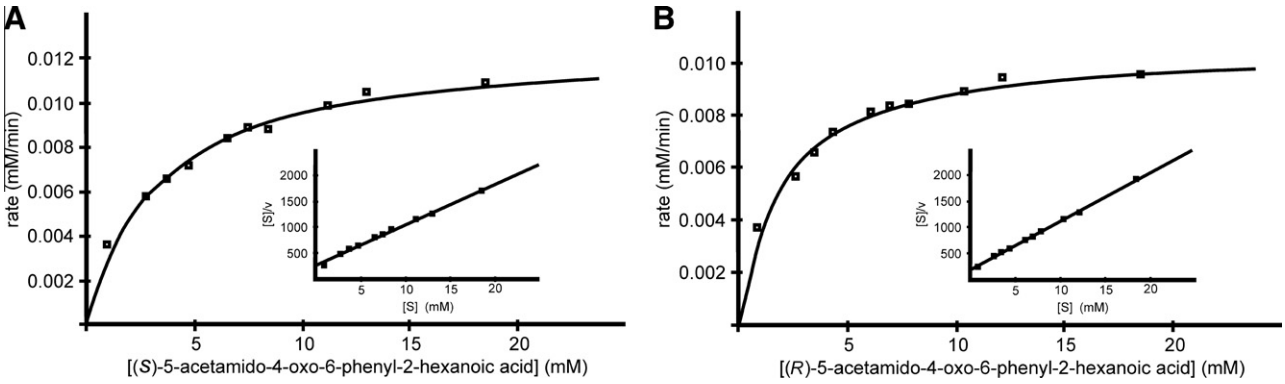

Figure 2. (A) Plot of rate of hydrolysis of methyl-(*S*)-5-acetamido-4-oxo-6-phenyl-2-hexenoic acid versus concentration, with Hanes–Woolf plot inset. K_M and V_{max} are 8.6 mM and 0.058 mM/min, respectively. (B) Plot of rate of hydrolysis of methyl-(*R*)-5-acetamido-4-oxo-6-phenyl-2-hexenoic acid versus concentration, with Hanes–Woolf plot inset. K_M and V_{max} are 6.1 mM and 0.048 mM/min, respectively.

the crystal structure, Amzel et al. use the notation Cu_M to refer to the copper ion at the substrate binding site which is ligated by one methionine residue and two histidines. We therefore first proceeded to demonstrate that docked *N*-Ac-L-Phe-Gly recapitulates the major interactions between substrate and enzyme that were observed in the crystal structure. As shown in Figure 3A, which illustrates an overlay of docked *N*-Ac-L-Phe-Gly onto the X-ray coordinates of the complex with *N*-Ac-3,5-diiodo-L-Tyr-Gly, this is indeed the case. As pointed out by Amzel et al., four major interactions are evident: (1) a salt bridge between the glycyl carboxylate of the ligand and the positively-charged guanidinium functionality of Arg240; (2) a variety of van der Waals' contacts, both between the main peptide chain of the substrate and the Cu_M ligands (Met314 and His242), and between the P_2 benzyl side chain and various residues of the large hydrophobic pocket of the active site (especially Phe112); (3) a hydrogen bond between the amide nitrogen of the substrate and the side-chain carbonyl group of Asn316; (4) a hydrogen bond between the substrate carboxylate and the phenol of Tyr318. It is evident from Figure 3A that all of these interactions are maintained in the case of *N*-Ac-L-Phe-Gly, and we calculate an rms deviation of 1.22 between our docked *N*-Ac-L-Phe-Gly and the crystal structure ligand. Moreover, the glycyl methylene of *N*-Ac-L-Phe-Gly is oriented such that the pro-(*S*) hydrogen is directed toward Cu_M, whereas the pro-(*R*) hydrogen is oriented away from Cu_M toward the interior of the hydrophobic pocket of the enzyme. This is consistent with the reaction stereospecificity of PAM, which abstracts only the pro-(*S*) hydrogen of peptide substrates and forms (*S*)-hydroxyglycines exclusively.[16]

In sharp contrast, as illustrated in Figure 3B, the substrate enantiomer, *N*-Ac-D-Phe-Gly does not closely associate with any PAM active site residues. Instead, as the simulation necessarily confines the ligand within the space outlined by the parameters of the docking box, this 'ligand' occupies the extensive available free space between Asn316, Lys134, and Leu206. This is consistent with our previous report[16] that *N*-Ac-D-Phe-Gly, is not a PAM substrate and exhibits only extremely weak binding (K_I = 1.3 mM) when evaluated as a potential inhibitor for the enzyme.

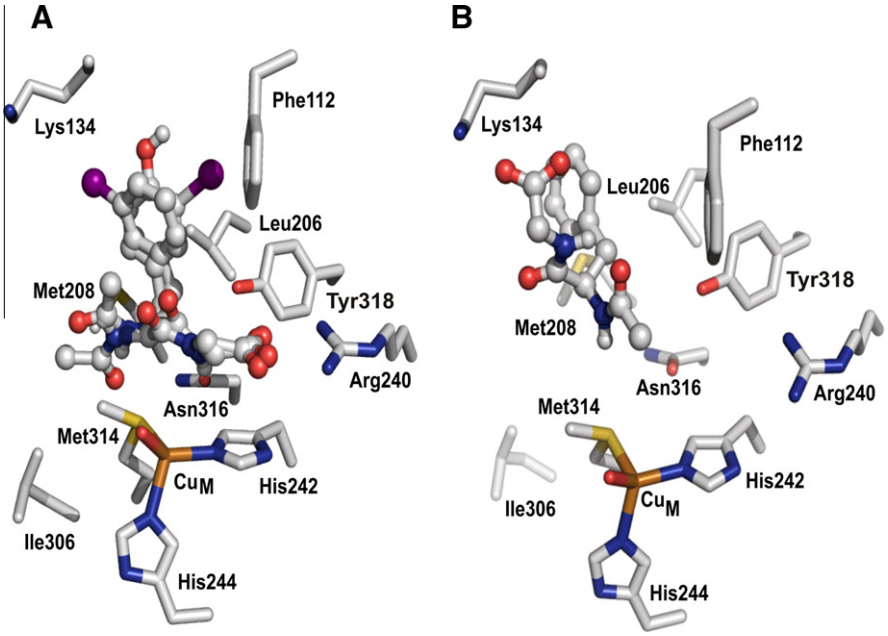

Figure 3. (A) *N*-Ac-L-Phe-Gly docked to PAM active site and overlaid with the crystal structure ligand *N*-Ac-L-2′,5′-diiodo-Tyr-Gly[24] to illustrate similarity in binding mode. *N*-Ac-L-Phe-Gly forms a bidentate salt bridge with Arg240, hydrogen bonds with Asn 316 and Tyr318, and the phenyl ring associates closely with Phe112. The pro-(*S*) hydrogen would be directed toward Cu_M. (B) *N*-Ac-D-Phe-Gly docked to PAM active site fails to bind or associate with Arg240, Phe112, or Tyr318. The carboxylate of the ligand is in proximity with the positively-charged amino group of Lys134.

2.3. Mechanism-based inhibitor enantiomers: (*S*)-AOPHA versus (*R*)-AOPHA

As shown in Figure 4A, the orientation of docked (*S*)-AOPHA is very similar overall to that of *N*-Ac-L-Phe-Gly. Again, the ligand carboxylate forms both a salt bridge with the guanidinium of Arg240 and a hydrogen bond with Tyr318, the phenyl ring of the ligand associates closely with Phe112, and the backbone is in VDW contact with Met314/His242. As shown in Figure 4B, these three binding interactions are still present for the olefinic enantiomer, (*R*)-AOPHA. The salt bridge to Arg240 and the hydrogen bond interaction with Tyr318 are both quite apparent. While the location of the phenyl ring differs from that in Figure 4A, a compensating hydrophobic interaction with Met208 is evident; the similar K_I values for the two enantiomers suggest that this effectively offsets the binding energy of the lost Phe112 association. Obviously, since the olefinic irreversible inhibitors possess an sp^2 carbon at the position of the amide nitrogen of PAM substrates, a substrate-type hydrogen bond interaction with Asn316 is not possible.

It is important to note that the olefinic moieties of both (*S*)- and (*R*)-AOPHA are well-positioned to undergo catalytic processing at the Cu_M center that gives rise to irreversible inhibition, as these atoms are nearly superimposable upon the homologous atoms of both our docked *N*-Ac-L-Phe-Gly and Amzel's crystal-structure ligand. Indeed, this is also the case for docked (*S*)-5-acetamido-7-methylthio-4-oxo-2-heptenoic acid (the methionine analog of AOPHA) and its (*R*)-enantiomer, shown in Figure 5A and B. Here again, the docked structures recapitulate the salt bridge with Arg240, the hydrogen bond with Tyr318, the protrusion of the P_2 side chain into the hydrophobic pocket, and the positioning of the olefinic functionality into close proximity with the Cu_M reaction center.

2.4. Reversible competitive inhibitors: *N*-Ac-L-Leu-OCH_2COOH versus *N*-Ac-D-Leu-OCH_2COOH

We have previously shown that the glycolate esters, *N*-Ac-L-Leu-OCH_2COOH and *N*-Ac-L-Phe-OCH_2COOH, are competitive inhibitors of PAM (K_I = 59.8 and 45.2 μM, respectively).[16] Docked *N*-Ac-L-Leu-OCH_2COOH (Fig. 6A) displays the aforementioned Arg240, Tyr318 and Phe112 interactions. The corresponding D-enantiomers of these esters, on the other hand, are very poor competitive inhibitors of PAM, with K_I values in excess of 2 mM. As illustrated in Figure 6B, *N*-Ac-D-Leu-OCH_2COOH, like *N*-Ac-D-Phe-Gly, does not dock productively within the confines of the PAM active site, instead occupying the largely empty space between Met208, Leu206, and Lys134. Thus, these docking results are fully consistent with the kinetic data for our glycolate-ester competitive inhibitors, which exhibit the same subsite stereospecificity as the substrates.

2.5. 'Un-natural' substrates: *O*-Ac-(*S*)-Mandelyl-Gly and *O*-Ac-(*R*)-Mandelyl-Gly

These two enantiomers are O-acetylated phenylglycine analogs of *N*-Ac-Phe-Gly. We have previously shown that *O*-Ac-(*S*)-Mandelyl-Gly is a PAM substrate, whereas its (*R*)-enantiomer is not.[16] Docked *O*-Ac-(*S*)-Mandelyl-Gly (Fig. 7A) displays the aforementioned Arg240, Tyr318 and Phe112 interactions. Due to the lack of the benzylic methylene relative to *N*-Ac-Phe-Gly, the *O*-Ac-(*S*)-Mandelyl-Gly is drawn upwards into the active site resulting in the formation of a hydrogen bond between the ligand's amide hydrogen and Tyr318, rather than Asn316. As a result, the ligand's main chain is no longer in van der Waals' contact with Met314 and His242; the loss of these interactions likely contributes to the greatly increased K_M value of *O*-Ac-(*S*)-Mandelyl-Gly (more than an order of magnitude greater than that of *N*-Ac-L-Phe-Gly; see Scheme 1). As with *N*-Ac-D-Phe-Gly, the stereotopically equivalent (*R*)-*O*-Ac-Mandelyl-Gly does not bind productively to the active site of the enzyme (Fig. 7B), with no hydrogen bonds forming between ligand and receptor, and no salt bridge formation between the substrate carboxylate and Arg240. Thus it is evident from both the kinetic data and the molecular docking studies that the change from an *N*-acetyl group to an *O*-acetyl group does not alter the stereoselectivity of PAM toward substrate enantiomers.

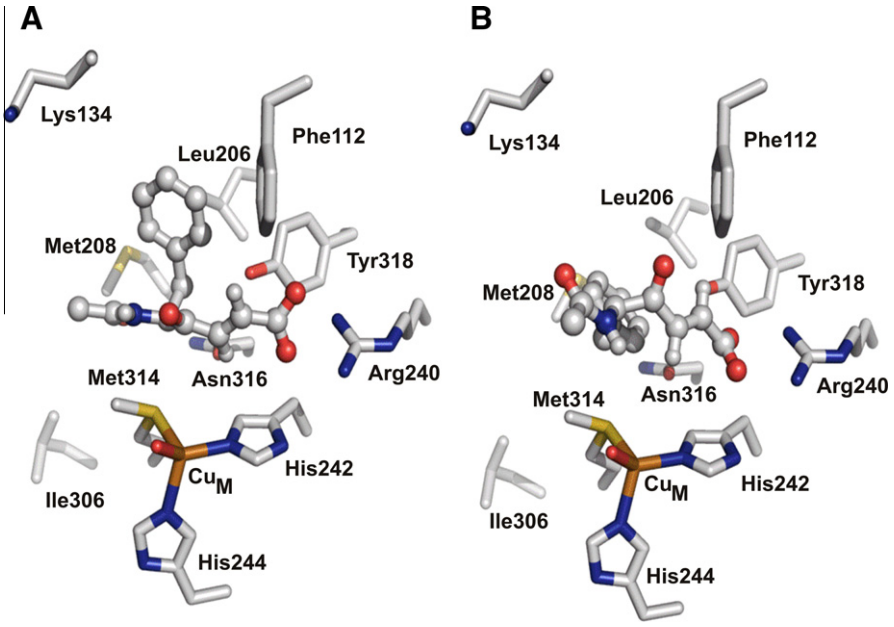

Figure 4. (A) (*S*)-5-Acetamido-4-oxo-6-phenyl-2-hexenoic acid docked to PAM active site adopts a conformation very similar to that of *N*-Ac-L-Phe-Gly, forming a salt bridge with Arg240, a hydrogen bond with Tyr318, and the phenyl ring of ligand in close proximity to Phe112. (B) (*R*)-5-Acetamido-4-oxo-6-phenyl-2-hexenoic acid docked to PAM active site has a salt-bridge formed with the guanidinium moiety of Arg240 and a hydrogen bond formed with Tyr318. The phenyl ring, unlike the L-enantiomer, although still directed into the hydrophobic pocket of the enzyme, associates closely with Met208 rather than Phe112.

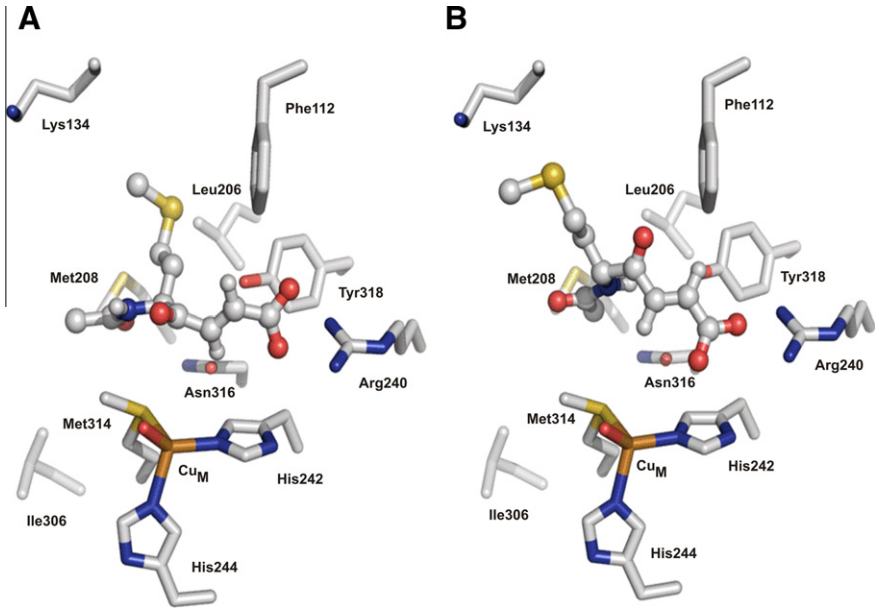

Figure 5. (A) (*S*)-5-Acetamido-7-methylthio-4-oxo-2-heptenoic acid docked to PAM active site, adopts a conformation similar to that of (*S*)-5-acetamido-4-oxo-6-phenyl-2-hexenoic acid. (B) (*R*)-5-Acetamido-7-methylthio-4-oxo-2-heptenoic acid docked to PAM active site, adopts a slightly different conformation in the methionyl side chain than that seen for (*R*)-5-acetamido-4-oxo-6-phenyl-2-hexenoic acid.

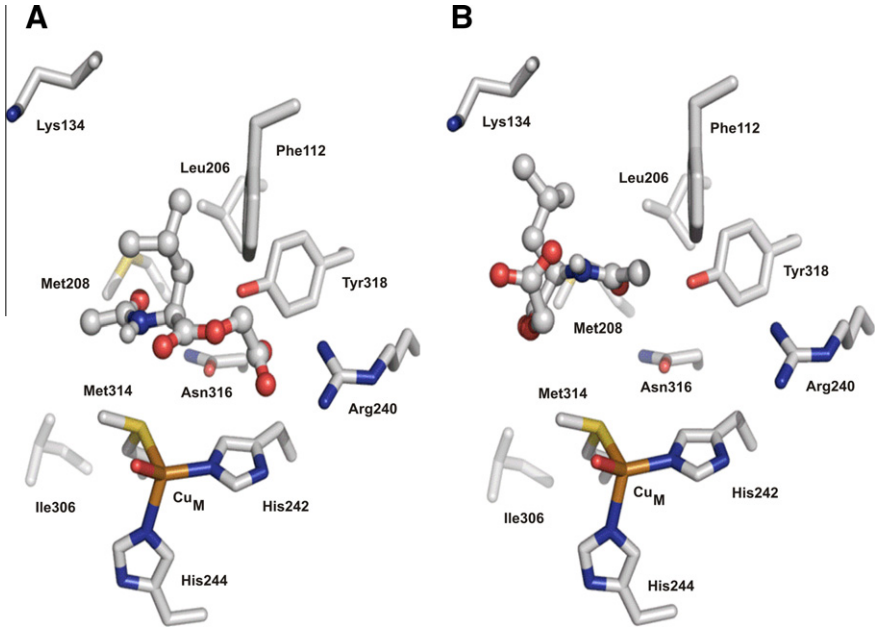

Figure 6. (A) *N*-Ac-L-Leu-OCH_2COOH docked to PAM active site. The carboxylate forms a salt bridge with Arg240 and the *sec*-butyl side chain occupies space in the hydrophobic pocket corresponding to that of the aromatic ring of *N*-Ac-L-Phe-Gly. (B) *N*-Ac-D-Leu-OCH_2COOH docked to the PAM active site. D-enantiomer is unable to bind productively to any active site residues, and fails to adopt an orientation characteristic of a substrate or competitive inhibitor.

3. Discussion

The results reported herein demonstrate that the inhibitory stereochemistry of olefinic mechanism-based irreversible amidation inhibitors differs from the strict subsite stereospecificity exhibited by PAM toward both substrates and reversible competitive inhibitors. To the best of our knowledge, there is only one other clear example in the literature where the stereospecificity of a particular enzyme toward mechanism-based irreversible inhibitors differs from that for substrates and competitive inhibitors. This example is the work of Kim et al.[23,24,31,25] on mechanism-based inhibitors of carboxypeptidase A (CPA) a zinc-containing metalloprotease which hydrolyzes C-terminal hydrophobic residues of L-configuration adjacent to P_2 residues also with an L-configuration (i.e., only one of four possible diastereomers). The molecule 2-benzyl-3,4-epoxybutanoic acid was designed as a mechanism-based inhibitor that alkylates the catalytic residue Glu270; unexpectedly, the (2*S*,3*R*)-isomer, with a reverse stereochemistry at the 2-position to that of the substrates, was found to be twice as potent as its (2*R*,3*S*)-enantiomer. Similarly, it was found that all four diastereomers of the related molecule α-benzyl-2-oxo-1,3-oxazolidine-4-acetic acid irreversibly inhibit CPA with comparable potency, in

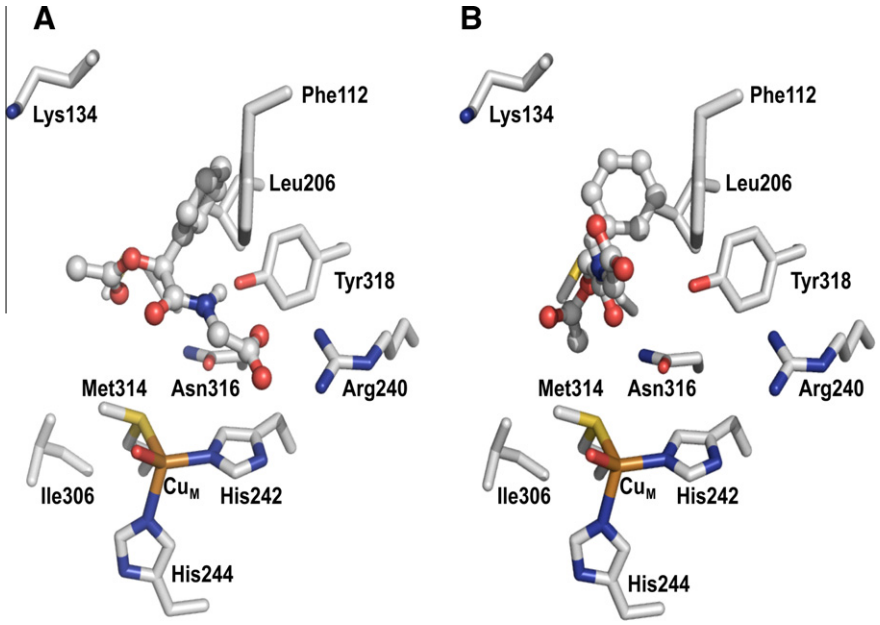

Figure 7. (A) *O*-Ac-(*S*)-Mandelyl-Gly docked to the PAM active site. Binds in a similar manner to PAM substrate *N*-Ac-L-Phe-Gly. The shorter P_2 side chain results in the molecule being pulled upwards toward Phe112, and two hydrogen bonds are formed with Tyr318. (B) *O*-Ac-(*R*)-Mandelyl-Gly docked to PAM. The molecule was unsuccessful in binding in the manner of substrate, competitive inhibitor or mechanism-based inhibitor.

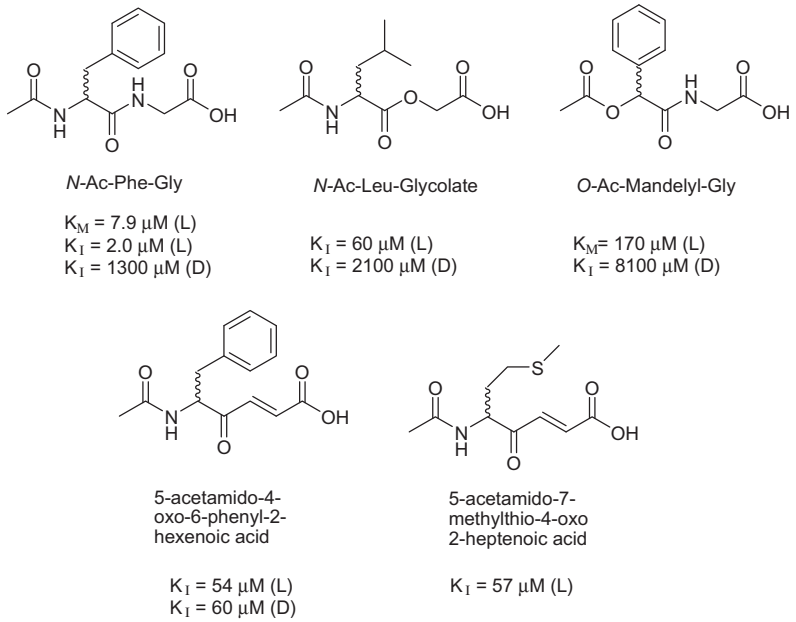

Scheme 1. Kinetic parameters of compounds used in molecular modeling studies.

contrast to the strict stereospecificity of CPA catalysis. Mechanistically, Kim et al. propose that for the oxazolidinone inhibitors, the Glu270 carboxylate attacks at the carbamate carbonyl rather than at the 5-position of the oxazolidinone ring. It should be noted that Moreira et al.[32] have reported an apparent lack of stereospecificity in the mechanism-based inhibition of human leukocyte elastase by oxazolidin-2,4-dione derivatives. However, since only the diastereomeric pairs were purified, it is unclear whether or not all four stereoisomers are active, although the authors' docking results suggested that only the (4*R*,5′*S*)- and (4*S*,5′*S*)-diastereomers, with chirality corresponding to that at the P1-position of normal substrates, are active.

Turning to reversible inhibitors, Fleet et al. have shown that the 'un-natural' enantiomers of a number of iminosugar glycomimetics are potent glucosidase inhibitors,[33–35] and these investigators have termed them 'looking-glass inhibitors'. For example, L-DMDP (2,5-dideoxy-2,5-imino-L-mannitol) was found to be 2–4 orders of magnitude more potent in inhibiting plant and mammalian α-glucosidases than its D-enantiomeric natural product. Similar results have been noted for a variety of natural product sugar analogs and their enantiomeric counterparts, such as L-DIM (1,4-dideoxy-1,4-imino-L-mannitol) and L-AB1 (1,4-dideoxy-1,4-imino-L-arabinitol). However, kinetic analyses of the L- and D-sugars proved that the unnatural 'looking-glass inhibitors' of DMPD

and AB1 actually exhibit non-competitive inhibition, as opposed to the competitive inhibition exhibited by the natural D-sugar analogs. The authors interpreted this as evidence that the 'unnatural' analogs actually bind to a site on the enzyme other than the active site.[36] More recently, these investigators have found that both enantiomers of *N*-benzyl-1,4-dideoxy-1,4-imino-lyxitol are moderate competitive inhibitors of α-D-galactosidase.[37] Similarly, Schramm et al. have found that for D- and L-immucillin, transition-state analog inhibitors of purine nucleoside phosphorylase, both L-5′-deaza-l′-aza-2′-deoxy-l′-(9-methylene)-immucillin-H and its 'natural' enantiomer are competitive inhibitors with K_I values differing by a factor of three.[38]

Several cellular kinases that are involved in the bioactivation of nucleoside pro-drugs, such as 2′,3′-dideoxy-3′-thiacytidine (lamivudine/3TC) and L-thymidine, into their active triphosphate forms have been shown to exhibit 'relaxed enantioselectivity'. In many of these cases, although the relevant substrates are chiral, stereoselectivity is very low and this feature also extends to very low enantioselectivity in the binding efficacy of competitive inhibitor nucleoside analogs. Thus, for example, cytosolic deoxycytidine kinase (dCK) and mitochondrial thymidine kinase (TK2) catalyze the phosphorylation of either 'un-natural' L-thymidine or D-thymidine to their respective monophosphates (L-TMP/D-TMP) with nearly equal facility,[39,40] and UMP/CMP kinase and TMP kinase generate diphosphate nucleotides with a similar lack of enantioselectivity.[41–43] Similarly, human 3-phosphoglycerate kinase (hPGK), perhaps the most well-studied of these kinases, is also non-specific toward its nucleotide substrates.[44,45] Finally, a variety of viral thymidine kinases, including those from Herpes Simplex I, Herpes Simplex 2, Pseudorabies, and Varicella zoster, coined as 'ambidextrous enzymes', have also been found to be promiscuous with respect to 'un-natural' L-thymidine.[46–49]

In the case of our olefinic irreversible inhibitors, the AOPHA enantiomers have three major points of contact with the active site of the enzyme: the salt bridge with Arg240, the hydrogen bond with Tyr318, and the close hydrophobic interactions with Phe112/Tyr318. Unlike the corresponding *N*-Ac-L-Phe-Gly substrate, the inclusion of the olefinic moiety results in the elimination of the hydrogen bond that would form between a peptide substrate and Asn316. We suggest that the lack of this hydrogen bond interaction with Asn316 gives rise to the loss of the subsite stereospecificity of the enzyme. Indeed, flexible alignment overlays confirm that both AOPHA enantiomers are able to closely overlay with *N*-Ac-L-Phe-Gly, whereas the substrate enantiomers themselves are poorly aligned at the glycine residue, and is evident from Figure 4 that the olefinic moieties of both (*S*)- and (*R*)-AOPHA are well-positioned to undergo the catalytic processing at the Cu_M center that gives rise to irreversible inhibition. Thus, our modeling results are remarkably consistent with the kinetic data for these mechanism-based irreversible inhibitors.

Amidation represents a potentially attractive target point for modulating the production of bioactive peptides and thereby affecting certain disease states. Amidated peptides such as substance P and calcitonin gene-related peptide are well established mediators of inflammation, and we have demonstrated that our irreversible amidation inhibitors exhibit potent anti-inflammatory activity against both acute and chronic inflammation in rats.[20,21] The proliferation of some tumor cells is dependent on autocrine growth loops that require amidated autocrine growth factors, and we have shown that an irreversible PAM inhibitor is selectively cytotoxic toward WB-Ras-transformed rat liver epithelial cells versus untransformed cells, and also restores gap-junctional communication in these transformed cells.[22] Since stereospecificity is a key aspect in the design of enzyme-targeted inhibitors, the results reported here should facilitate the future development of new classes of amidation inhibitors with therapeutic potential.

4. Experimental

4.1. Synthesis of (*R*)-5-acetamido-4-oxo-6-phenyl-2-hexenoic acid

4.1.1. *N*-Ac-D-Phe-OMe

In a 100 mL round-bottomed flask 9.4 mL (120 mmol) pyridine and 11.0 mL (120 mmol) acetic anhydride were combined at 0 °C. Next, 5.0 g (23 mmol) D-Phe-OMe HCl was dissolved in the above solution and the ice bath was removed. The reaction was allowed to proceed overnight at room temperature, turning a rich purple color. The reaction was quenched by the addition of 100 mL water/ice slurry. The resulting solution was again allowed to return to room temperature and then extracted four times with CH_2Cl_2. The extracts were pooled and then rinsed three times each with saturated $NaHCO_3$ solution, 0.1 M HCl solution, and water. The methylene chloride solution was dried over $MgSO_4$ and evaporated to dryness under reduced pressure, yielding 4.5 g (20 mmol, 87%) of *N*-Ac-D-Phe-OMe as a white solid. ^{1}H NMR ([^{2}H]chloroform, tetramethylsilane (TMS) = 0.0 ppm): δ 1.98 (s, 3H), δ 3.12 (m, 2H), δ 3.73 (s, 3H), δ 4.89 (m, 1H), δ 5.90 (broad, 1H), δ 7.09 (m, 2H), δ 7.27 (m, 3H).

4.1.2. *N*-Ac-D-Phe-α-ketophosphonate

In a 3-necked 250 mL round-bottomed flask at −78 °C under argon, 4.4 mL (41 mmol) dimethylmethylphosphonate was added to 45 mL dry THF (dried over sodium metal). Next, 16.5 mL of *n*-BuLi (2.5 M in hexanes, 42 mmol) was added dropwise over 30 min. A small quantity of white precipitate formed, which disappeared over 15 min. Next, 4.5 g (20 mmol) *N*-Ac-D-Phe-OMe in 50 mL dry THF were added all at once. The reaction was allowed to proceed overnight and return to room temperature, turning yellow-orange. The reaction mixture was quenched by the addition of 100 mL water and washed twice with 50 mL diethyl ether. The aqueous layer was acidified by 0.1 M HCl (pH 1.0), and then extracted four times with 50 mL CH_2Cl_2. The methylene chloride extracts were pooled, dried over $MgSO_4$, and evaporated to dryness under reduced pressure, yielding a crude yellow oil. The crude *N*-Ac-D-Phe-α-ketophosphonate was purified by silica gel chromatography from chloroform/methanol (20:1 v/v) yielding 6.1 g yellow oil (19 mmol, 95%). ^{1}H NMR ([^{2}H]chloroform, TMS = 0.0 ppm): δ 1.98 (s, 3H), δ 2.98–3.30 (m, 4H), δ 3.72–3.78 (m, 6H), δ 4.82–4.94 (q, 1H), δ 6.52 (d, 1H), δ 7.10–7.32 (m, 5H).

4.1.3. Methyl glyoxylate

First, 3.6 g (39 mmol) glyoxylic acid monohydrate and 100 mg *p*-toluenesulfonic acid were dissolved in 4.6 mL (29 mmol) methyl dimethoxyacetate in a 100 mL round-bottomed flask. The reaction mixture was heated at reflux overnight. The next morning, the reaction mixture was cooled to room temperature and 4 g phosphorus pentoxide were slowly added. The reaction mixture was again heated at reflux (80 °C) for 4 h, allowed to cool to room temperature and then distilled under reduced pressure. The product which distilled at 70 °C was collected (3.0 mL) as a yellow oil. ^{1}H NMR ([^{2}H]chloroform, TMS = 0.0 ppm) δ 3.76 (singlet).

4.1.4. Methyl-(*R*)-5-acetamido-4-oxo-6-phenyl-2-hexenoic acid

At first, 6.1 g (19 mmol) *N*-Ac-D-Phe-α-ketophophonate were placed in a 100 mL round-bottomed flask over ice. Next, 10 mL water and 2.5 mL methyl glyoxylate were added, and after 5 min 20 mL of potassium carbonate solution (0.25 g/mL) were added. A white precipitate formed immediately upon the addition of the carbonate solution. The reaction was allowed to proceed for 30 min. The white solid was collected by vacuum filtration, rinsed with cold water, and recrystallized from ethanol/water. The white solid was again collected by vacuum filtration and dried under vacuum over

phosphorus pentoxide (1.1 g, 19%). ^{1}H NMR ([^{2}H]chloroform, TMS = 0.0 ppm) δ 1.98 (s, 3H), δ 3.00–3.22 (m, 2H), δ 3.80 (s, 3H), δ 5.05–5.12 (q, 1H), δ 6.04 (br s, 1H), δ 6.76 (d, 1H, J = 15.9 Hz), δ 7.05 (m, 2H), δ 7.12 (d, 1H, J = 15.9 Hz), δ 7.25 (m, 3H).

4.1.5. (*R*)-5-Acetamido-4-oxo-6-phenyl-2-hexenoic acid

Typically, 100 mg (0.4 mmol) methyl-(*R*)-AOPHA was dissolved in 8 mL EtOH, and slowly added to 40 mL 100 mM TRIS buffer (pH 7.1) at 37 °C. To initiate the reaction, 100 μL of 6 mg/mL reconstituted pig liver esterase (E.C. 3.1.1.1, 15 U/mg) was added. The reaction was monitored on a C8 Alltech Allsphere column at 260 nm (25.0% CH_3CN/74.9% water/0.1% TFA) at a flow rate of 1.5 mL/min. The reaction went to >99% completion after 24 h. The reaction mixture was ultrafiltered through an Amicon YM-10 membrane, the filtrate was acidified (pH 2.0) by addition of 0.1 M HCl, and extracted four times with 10 mL EtOAc, dried over $MgSO_4$, and evaporated under reduced pressure to yield 80 mg (0.3 mmol, 75%) white solid. RP-HPLC analysis indicates purity of greater than 99%. ^{1}H NMR (DMSO-d_6, DMSO = 2.49 ppm): δ 1.78 (s, 3H), δ 2.71–3.08 (m, 2H), δ 4.72 (m, 1H), δ 6.54 (d, 1H, J = 15.9 Hz), δ 7.06 (d, 1H, J = 15.9 Hz), δ 7.21 (m, 5H), δ 8.41 (d, 1H). Polarimetry: $[\alpha]_D^{25} = 12.5 \pm 1.4$ (c 0.10, MeOH).

4.2. Synthesis of (*S*)-5-acetamido-7-methylthio-4-oxo-2-heptenoic acid

4.2.1. *N*-Ac-L-Met-OMe

In a typical reaction, 73 mL of acetic anhydride (780 mmol) and 63 mL pyridine (780 mmol) were combined in a round-bottomed flask and chilled on ice. After 5–10 min, 8.6 g (100 mmol) L-methionine methyl ester HCl were added and the reaction mixture was allowed to slowly return to room temperature overnight. The next morning, the reaction was quenched with cold water and extracted four times with 75 mL of methylene chloride. The extracts were then rinsed three times each with 1 M HCl, saturated sodium bicarbonate solution, and water. The extracts were then dried over $MgSO_4$, filtered, and evaporated under reduced pressure, yielding a yellow oil which crystallized upon standing. The crude product was recrystallized in ethyl ether at −20 °C. Crystals (19.3 g, 94 mmol, 94%) were isolated by vacuum filtration. Mp = 41.7–42.4 °C. ^{1}H NMR ([^{2}H]-chloroform, TMS = 0.0 ppm): δ 1.86–2.20 (m, 2H), δ 2.00 (s, 3H), δ 2.05 (s, 3H), δ 2.45–2.60 (m, 2H), δ 3.75 (s, 3H), δ 4.62–4.70 (m, 1H), δ 6.13–6.19 (bd, 1H).

4.2.2. *N*-Ac-L-Met-α-ketophosphonate

At first, *N*-Ac-L-Met-OMe was dried in a vacuum desiccator over P_2O_5 flushed with argon gas. In a three-neck round-bottomed flask under argon pressure, 11.0 mL *n*-butyllithium (2.5 M in hexanes, 28.0 mmol) was added dropwise to 3.4 mL dimethylmethylphosphonate (32.0 mmol) in 100 mL dried, distilled tetrahydrofuran at −78 °C, and allowed to stand for 15 min, upon which a white precipitate formed. Then, 2.8 g (14.0 mmol) *N*-Ac-L-Met-OMe dissolved in 50 mL THF were added all at once. The reaction was allowed to return to room temperature (15 h) and quenched with 100 mL water. Reaction mixture was rinsed twice with 100 mL ethyl ether, acidified with dilute HCl to pH 1.0, and extracted three times with 50 mL methylene chloride. Extracts were combined, dried over magnesium sulfate, and evaporated under reduced pressure to yield 4.0 g of a yellow oil (13.5 mmol, 96%). ^{1}H NMR ([^{2}H]-chloroform, TMS = 0.0 ppm): δ 1.75–2.20 (m, 2H), δ 2.00 (s, 3H), δ 2.02–2.10 (s, 3H), δ 3.05–3.38 (m, 4H), δ 3.62–3.78 (m, 6H), δ 4.61–4.72 (m, 1H), δ 7.09–7.20 (bd, 1H). MS (ESI+): 298 (M+1).

4.2.3. Methyl-(*S*)-5-acetamido-7-methylthio-4-oxo-2-heptenoic acid

First, 1.5 g (5.0 mmol) *N*-Ac-L-Met-α-ketophosphonate were combined with 0.5 g (5.7 mmol) methyl glyoxylate (synthesis described above) and allowed to stir on ice for 5–10 min. Then, 6 mL potassium carbonate (20% w/v) was added to initiate the reaction. A yellow precipitate formed immediately. The precipitate was collected by vacuum filtration, and washed with water and ethyl ether, yielding 0.70 g (2.7 mmol, 54%) off-white crystals. Mp = 104–106 °C. ^{1}H NMR ([^{2}H]-chloroform, TMS = 0.0 ppm): δ 1.80–2.29 (m, 2H), δ 2.05–2.07 (s, 3H), δ 2.08–2.12 (s, 3H), δ 2.45–2.58 (m, 2H), δ 3.82 (s, 3H), δ 4.95–5.10 (m, 1H), δ 6.30–6.40 (bd, 1H), δ 6.80–8.90 (d, 1H), δ 7.22–7.28 (d, 1H). MS (ESI+): 260 (M+1).

4.2.4. (*S*)-5-Acetamido-7-methylthio-4-oxo-2-heptenoic acid

Crude ester, 1.8 g (6.9 mmol), was dissolved in a minimal amount, (≈10 mL) of CH_3CH_2OH. The dissolved sample was then slowly added to 250 mL 100 mM Tris–Cl buffer, pH 7.3. The reaction was initiated by the addition of 0.0065 g reconstituted porcine liver esterase (E.C. 3.1.1.1, lyophile, >15 U/mL) and incubated at 37 °C. After several hours a finely dispersed precipitate was formed. The reaction was monitored by RP-HPLC at a wavelength of 214 nm on an Alltech Allsphere C-8 column, using a mobile phase of 15.0% ACN:84.9% H_2O:0.1% TFA at a flow rate of 1.5 mL/min. The reaction was allowed to progress until the substrate peak had disappeared completely, with the concomitant formation of a new peak representing the free acid. Retention times for the ester and the product acid were 21 and 6 min, respectively. The reaction mixture was ultrafiltered using an Amicon YM-10 membrane. The filtrate was rinsed three times with 50 mL Et_2O, acidified to a pH of 1.0 with HCl, extracted four times with 50 mL CH_2Cl_2, dried over $MgSO_4$, filtered, and evaporated under reduced pressure to yield a white solid. Recrystallized from methylene chloride and isolated by vacuum filtration to yield 0.7 g white solid (2.9 mmol, 42%). The product was analyzed by NMR and ESI Mass Spectrometry. Purity was greater than 99%, as determined by RP-HPLC. ^{1}H NMR ([^{2}H]-DMSO-d_6, DMSO = 2.49 ppm): δ 1.64–2.0 (m, 2H), δ 2.82 (s, 3H), δ 2.00 (s, 3H), δ 2.40–2.55 (m, 2H), δ 4.52–4.60 (m, 1H), δ 6.57–6.62 (d, 1H), δ 7.00–7.07 (d, 1H), δ 8.35–8.40 (bd, 1H). MS (ESI+): 246 (M+1).

4.3. Synthesis of TNP-D-Tyr-L-Val-Gly (TNP-YVG)

The synthesis of TNP-YVG was carried out according to previously described procedures.[50] Briefly, 12 mg 2–4-6-trinitrobenzenesulfonic acid hydrate and 11 mg D-Tyr-Val-Gly were dissolved in 20 mL of MeOH/water (1:4) in a foil-wrapped round-bottomed flask. The reaction was initiated via the addition of three drops of Et_3N, upon which the reaction mixture turned a deep orange. After 30 min, 100 mL water was added and the reaction mixture was acidified to pH 2.0 by the addition of 0.1 M HCl, turning yellow. The reaction mixture was extracted three times with 25 mL EtOAc, and the extracts were pooled, dried over $MgSO_4$, and evaporated to dryness under reduced pressure. The residue was dissolved in a minimum volume of 1:1 Et_2O/EtOAc, and hexanes were added until the solution turned cloudy. After storing overnight at −20 °C, the yellow precipitate was collected by vacuum filtration, dissolved in approximately 5 mL of MeOH, and stored at −70 °C. Concentration was determined by UV–vis spectroscopy. The extinction coefficient of TNP-YVG is 12.2×10^3 at 350 nm. A yield of 50% is typical for this synthesis. RP-HPLC analysis revealed no impurities.

4.4. Synthesis of (*S*)-5-acetamido-4-oxo-6-phenyl-2-hexenoic acid

This compound was synthesized using the previously described procedure.[17]

4.5. Chiral HPLC chromatography

Chiral separations of the enantiomers of 5-acetamido-4-oxo-6-phenyl-2-hexenoic acid and methyl 5-acetamido-4-oxo-6-phenyl-2-hexenoate were carried out on a Phenomenex (D)-Penicillamine column. All compounds were dissolved in HPLC-grade methanol prior to injection. Absorbance was monitored at 260 nm on a Waters LC-Module 1 Plus. The mobile phase was 74.5:25:0.5 3 M $CuSO_4$/methanol/trifluoroacetic acid. Flow rate was 1.0 mL/min.

4.6. Expression of *X. Laevis* skin AE-1

Suspension cultures of Sf9 cells were treated with a Baculovirus Expression Vector (BEV) containing the gene for AE-1 created by Nishikawa et al.[51] Cells were counted via a hemocytometer and infected at 10 plaque-forming units per cell. Briefly, the cell suspension was centrifuged at low speeds to pellet the Sf9 cells, which were then resuspended with the appropriate volume of virus solution. Cells were incubated for 1 h with end-over-end rocking and Ex-Cell medium was added such that the final cell concentration was approximately 1×10^6 cells/mL. Cells were incubated in suspension culture for five days and then harvested by Fast Protein Liquid Chromatography (FPLC).

4.7. Enzyme isolation

First, AE-I was isolated from Sf9 suspension-cultured medium using a procedure developed by Suzuki.[51] and modified by Feng.[17] Typical starting volumes were 500 mL to 1 L. Cells were pelleted by low-speed centrifugation. The supernatant was loaded onto a Substance P-Sepharose Fast Flow cation-exchange column (2.6×40 cm, Pharmacia) equilibrated with 50 mM MES-sodium, pH 6.2. After the medium was loaded, the column was eluted for 120 min at a flow-rate of 1.5 mL/min to remove non-adsorbed material. The column was then eluted with a step-wise NaCl gradient: 0–150 mM NaCl over 30 min, 150–250 mM NaCl over 200 min, 250–500 mM NaCl over 50 min, and 500 mM NaCl for 300 min. Fractions were assayed for PAM activity by the procedure given below. Fractions with activity were pooled and concentrated over a 10,000 molecular-weight Amicon YM-10 membrane, and the buffer was exchanged to 50 mM Tris–Cl, pH 8.5 buffer.

The concentrated AE-1 solution was then applied to a MonoQ HR 10/10 column (Pharmacia) equilibrated with 50 mM Tris–Cl, pH 8.5 buffer. The column was washed for 30 min at 1.0 mL/min with starting buffer, and then eluted with a step-wise NaCl gradient: 0–50 mM NaCl for 15 min, 50–200 mM NaCl over 90 min, 200–500 mM NaCl over 30 min, and 500 mM NaCl for 30 min. Fractions with PAM activity were pooled and concentrated over an Amicon YM-10 membrane and applied to a Superose-12 HR 10/30 gel-filtration column (Pharmacia). Activity was eluted with HEPES pH 7.0 at a flow-rate of 0.5 mL/min for 90 min. Purified AE-1 eluted as a single peak over several fractions. Activity was pooled and concentrated, and stored as a 1:1 buffer/ethylene glycol solution at −20 °C. Activity is expressed in mU/mL, where 1 U is the amount of enzyme required to produce 1 μM TNP-YV(OH)G per minute at 37 °C.

4.8. PAM activity assay

Briefly, the assay solution contains 1 mg/mL catalase, 4 mM ascorbic acid, 4 μM copper sulfate, and 35 μM TNP-YVG in 250 μL 50 mM MES-Na, pH 6.5 at 37 °C. The conversion of TNP-YVG to TNP-YV(OH)G was kept to under 30% in order to obtain consistent initial rates. The reaction was quenched by the addition of 10% v/v 3 M $HClO_4$. Samples were centrifuged at 10,000 g for 30 min and the supernatant was assayed by RP-HPLC. Product concentrations were determined by RP-HPLC analysis on an Alltech Allsphere C8 column (250×4.2 mm, 5 μm particle size) with an authentic product standard curve. Mobile phase was 44.0:55.9:0.1 acetonitrile–water–trifluoroacetic acid at a flow rate of 1.5 mL/min. Absorbance was measured at 344 nm.

4.9. Dilution assay

Purified PAM was initially incubated in the above assay solution (37 °C), in the absence of TNP-YVG substrate, but in the presence of various concentrations of Triton X-100 and 80 mM KI. Inhibition reactions were initiated by the addition of purified PAM. Aliquots of 10 μL were withdrawn over an appropriate time course and reincubated in the standard PAM assay solution described above, containing saturating concentrations of TNP-YVG (50 μM), 0.1% v/v Triton X-100, and 80 mM KI. The reactions were quenched after 30 min and analyzed as described above. Residual PAM activity was measured as % initial activity of untreated control enzyme.

4.10. Progress curve inhibition kinetics

Purified PAM was incubated in the presence of varying concentrations of TNP-YVG (2.0–15 μM) and the appropriate inhibitor species (20–100 μM) in 5 mL of the standard PAM assay solution containing 0.1% v/v Triton X-100 and 80 mM KI. The reaction was initiated by the addition of enzyme and 250 μL aliquots were removed every minute, quenched with 10% v/v 3 M $HClO_4$, centrifuged, and the supernatant was analyzed for product concentration according to the chromatographic conditions described above.

4.11. PAM/ligand docking

All simulations were run using Molecular Operating Environment (MOE) software, Chemical Computing Group, Inc. (Montreal, Canada). Additional code 'more_dock.svl' was obtained from the SVL Exchange website (http://svl.chemcomp.com). All ligands were constructed using the MOE Builder module and built from the crystal-structure coordinates of the side-chain phenyl ring of the 1OPM ligand IYG,[24] thereby placing the side chains of all ligands in the hydrophobic pocket of the enzyme at the start of each docking run. Polar hydrogens were added to the ligands (including sp^2 hydrogens) and each ligand was minimized using the Engh–Huber force field with default parameters and 'solvation' enabled. Non-bonded and bonded cutoffs were changed to 5.5 and 4.5 Å, respectively.

The receptor used for molecular docking was the oxidized PAM crystal structure, 1OPM.[30] All water molecules, carbohydrates, and metal ions except for Cu_H and Cu_M were deleted from the receptor prior to molecular docking. Polar hydrogen atoms were added to the PAM crystal structure receptor, heavy atoms were locked, and the structure was energy-minimized using the Engh–Huber force field. Default energy parameters were used for the minimization and 'solvation' was enabled. Non-bonded and bonded cutoffs were changed, as for the ligand minimization, to 5.5 and 4.5 Å, respectively.

Docking simulations were performed using the Simulated Annealing algorithm (Engh–Huber force field), with all default parameters except that 'solvation' was enabled and the non-bonded and bonded cutoffs were changed to 5.5 and 4.5 Å, respectively. The docking box was centered at $40.4032 \times 25.3060 \times 40.4527$ (x,y,z) of the crystal structure receptor and had arbitrary dimensions of $60 \times 60 \times 60$ (x,y,z). All residues that were at least partially within the confines of the docking box were selected, and then all residues within 5.5 Å (the non-bonded cutoff) of those residues were selected. All other atoms were deleted. Minimized ligands were then subjected to a non-random start

simulation, and all bonds that are able to undergo rotation were allowed to deviate continuously ±30° from the minimized configuration. Initial temperatures were 1000 K. Typically, twenty-five runs were performed for each ligand, resulting in 25 docked conformations per ligand. Each run included six cycles of decreasing initial temperature, with 8000 iterations per cycle. Top scorers were determined from the electrostatic and van der Waals' energy contributions.

Acknowledgments

We gratefully acknowledge the partial support of this work by the National Institutes of Health (GM40540). We also gratefully acknowledge Mrs. Maggie Schwab Gunnerson for her contributions to the synthesis of the methionyl derivative.

References

1. Bradbury, A. F.; Smyth, D. G. *Eur. J. Biochem.* **1987**, *169*, 579–584.
2. Bradbury, A. F.; Smyth, D. G. *Biosci. Rep.* **1987**, *7*, 907–916.
3. Eipper, B. A.; Mains, R. E. *Annu. Rev. Physiol.* **1988**, *50*, 333–344.
4. Eipper, B. A.; Stoffers, D. A.; Mains, R. E. *Annu. Rev. Neurosci.* **1992**, *15*, 57–85.
5. Kato, I.; Yonekura, H.; Tajima, M.; Yanagi, M.; Yamamoto, H.; Okamoto, H. *Biochem. Biophys. Res. Commun.* **1990**, *172*, 197–203.
6. Katopodis, A. G.; May, S. W. *Biochemistry* **1990**, *29*, 4541–4548.
7. Katopodis, A. G.; Ping, D.; Smith, C. E.; May, S. W. *Biochemistry* **1991**, *30*, 6189–6194.
8. Perkins, S. N.; Husten, E. J.; Eipper, B. A. *Biochem. Biophys. Res. Commun.* **1990**, *171*, 926–932.
9. Ping, D.; Katopodis, A. G.; May, S. W. *J. Am. Chem. Soc.* **1992**, *114*, 3998–4000.
10. Tajima, M.; Iida, T.; Yoshida, S.; Komatsu, K.; Namba, R.; Yanagi, M.; Noguchi, M.; Okamoto, H. *J. Biol. Chem.* **1990**, *265*, 9602–9605.
11. Takahashi, K.; Okamoto, H.; Seino, H.; Noguchi, M. *Biochem. Biophys. Res. Commun.* **1990**, *169*, 524–530.
12. Bradbury, A. F.; Finnie, M. D. A.; Smyth, D. G. *Nature* **1982**, *298*, 686–688.
13. Eipper, B. A.; Mains, R. E.; Glembotski, C. C. *Proc. Natl. Acad. Sci. U.S.A.* **1983**, *80*, 5144–5148.
14. Ramer, S. E.; Cheng, H.; Palcic, M. M.; Vederas, J. C. *J. Am. Chem. Soc.* **1988**, *110*, 8526–8532.
15. Bradbury, A. F.; Smyth, D. G. *Biochem. Biophys. Res. Commun.* **1983**, *112*, 372–377.
16. Ping, D.; Mounier, C. E.; May, S. W. *J. Biol. Chem.* **1995**, *270*, 29250–29255.
17. Feng, J.; Shi, J.; Sirimanne, S. R.; Mounier-Lee, C. E.; May, S. W. *Biochem. J.* **2000**, *350*, 521–530.
18. Mounier, C. E.; Shi, J.; Sirimanne, S. R.; Chen, B. H.; Moore, A. B.; Gill-Woznichak, M. M.; Ping, D.; May, S. W. *J. Biol. Chem.* **1997**, *272*, 5016–5023.
19. Moore, A. B.; May, S. W. *Biochem. J.* **1999**, *341*, 33–40.
20. Bauer, J. D.; Sunman, J. A.; Foster, M. S.; Thompson, J. R.; Ogonowski, A. A.; Cutler, S. J.; May, S. W.; Pollock, S. H. *J. Pharmacol. Exp. Ther.* **2007**, *320*, 1171–1177.
21. Ogonowski, A. A.; May, S. W.; Moore, A. B.; Barrett, L. T.; O'Bryant, C. L.; Pollock, S. H. *J. Pharmacol. Exp. Ther.* **1997**, *280*, 846–853.
22. Sunman, J. A.; Foster, M. S.; Folse, S. L.; May, S. W.; Matesic, D. F. *Mol. Carcinog.* **2004**, *41*, 231–246.
23. Chung, S. J.; Chung, S.; Lee, H. S.; Kim, E. J.; Oh, K. S.; Choi, H. S.; Kim, K. S.; Kim, Y. J.; Hahn, J. H.; Kim, D. H. *J. Org. Chem.* **2001**, *66*, 6462–6471.
24. Kim, D. H. *Mini-Rev. Med. Chem.* **2001**, *1*, 155–161.
25. Lee, S. S.; Li, Z.-H.; Lee, D. H.; Kim, D. H. *J. Chem. Soc., Perkin Trans. 1* **1995**, 2877–2882.
26. Wang, Z. X.; Tsou, C. L. *J. Theor. Biol.* **1990**, *142*, 531–549.
27. Wang, Z. X. *J. Theor. Biol.* **1990**, *147*, 497–508.
28. Tsou, C. L. *Adv. Enzymol. Relat. Areas Mol. Biol.* **1988**, *61*, 381–436.
29. Wilson, W. B. S.; Barber, Y.; Scallen, T.; Morrow, C. *J. Org. Chem.* **1983**, *48*, 3960–3966.
30. Prigge, S. T.; Kolhekar, A. S.; Eipper, B. A.; Mains, R. E.; Amzel, L. M. *Science* **1997**, *278*, 1300–1305.
31. Kim, D. H. *Curr. Top. Med. Chem.* **2004**, *4*, 1217–1226.
32. Moreira, R.; Santana, A. B.; Iley, J.; Neres, J.; Douglas, K. T.; Horton, P. N.; Hursthouse, M. B. *J. Med. Chem.* **2005**, *48*, 4861–4870.
33. Fleet, G. W. J.; Nicholas, S. J.; Smith, P. W.; Evans, S. V.; Fellows, L. E.; Nash, R. J. *Tetrahedron Lett.* **1985**, *26*, 3127–3130.
34. Hakansson, A. E.; van Ameijde, J.; Guglielmini, L.; Horne, G.; Nash, R. J.; Evinson, E. L.; Kato, A.; Fleet, G. W. J. *Tetrahedron: Asymmetry* **2007**, *18*, 282–289.
35. Yu, C. Y.; Asano, N.; Ikeda, K.; Wang, M. X.; Butters, T. D.; Wormald, M. R.; Dwek, R. A.; Winters, A. L.; Nash, R. J.; Fleet, G. W. *Chem. Commun.* **2004**, 1936–1937.
36. Asano, N.; Ikeda, K.; Yu, L.; Kato, A.; Takebayashi, K.; Adachi, I.; Kato, I.; Ouchi, H.; Takahata, H.; Fleet, G. W. J. *Tetrahedron: Asymmetry* **2005**, *16*, 223–229.
37. Mercer, T.; Jenkinson, S.; Bartholemew, B.; Nash, R.; Miyauchi, S.; Kato, A.; Fleet, G. *Tetrahedron: Asymmetry* **2009**, *20*, 2368–2373.
38. Rinaldo-Matthis, A.; Murkin, A. S.; Ramagopal, U. A.; Clinch, K.; Mee, S. P.; Evans, G. B.; Tyler, P. C.; Furneaux, R. H.; Almo, S. C.; Schramm, V. L. *J. Am. Chem. Soc.* **2008**, *130*, 842–844.
39. Sabini, E.; Hazra, S.; Konrad, M.; Burley, S.; Lavie, A. *Nucleic Acids Res.* **2007**, *35*, 186–192.
40. Sabini, E.; Hazra, S.; Konrad, M.; Lavie, A. *J. Med. Chem.* **2007**, *50*, 3004–3014.
41. Ostermann, N.; Segura-Pena, D.; Meier, C.; Veit, T.; Monnerjahn, C.; Konrad, M.; Lavie, A. *Biochemistry* **2003**, *42*, 2568–2577.
42. Pasti, C.; Gallois-Montbrun, S.; Munier-Lehmann, H.; Veron, M.; Gilles, A. M.; Deville-Bonne, D. *Eur. J. Biochem.* **2003**, *270*, 1784–1790.
43. Alexandre, J. A.; Roy, B.; Topalis, D.; Pochet, S.; Perigaud, C.; Deville-Bonne, D. *Nucleic Acids Res.* **2007**, *35*, 4895–4904.
44. Gondeau, C.; Chaloin, L.; Lallemand, P.; Roy, B.; Perigaud, C.; Barman, T.; Varga, A.; Vas, M.; Lionne, C.; Arold, S. T. *Nucleic Acids Res.* **2008**, *36*, 3620–3629.
45. Varga, A.; Lionne, C.; Lallemand, P.; Szabo, J.; Adamek, N.; Valentin, C.; Vas, M.; Barman, T.; Chaloin, L. *Biochemistry* **2009**, *48*, 6998–7008.
46. Focher, F.; Maga, G.; Bendiscioli, A.; Capobianco, M.; Colonna, F.; Garbesi, A.; Spadari, S. *Nucleic Acids Res.* **1995**, *23*, 2840–2847.
47. Magrassi, L.; Finocchiaro, G.; Milanesi, G.; Benvenuto, F.; Spadari, S.; Focher, F. *Gene Ther.* **2003**, *10*, 2052–2058.
48. Spadari, S.; Maga, G.; Focher, F.; Ciarrocchi, G.; Manservigi, R.; Arcamone, F.; Capobianco, M.; Carcuro, A.; Colonna, F.; Iotti, S.; Garbesi, A. *J. Med. Chem.* **1992**, *35*, 4214–4220.
49. Spadari, S.; Maga, G.; Verri, A.; Bendiscioli, A.; Tondelli, L.; Capobianco, M.; Colonna, F.; Garbesi, A.; Focher, F. *Biochimie* **1995**, *77*, 861–867.
50. Katopodis, A. G.; May, S. W. *Biochem. Biophys. Res. Commun.* **1988**, *151*, 499–505.
51. Suzuki, K.; Shimoi, H.; Iwasaki, Y.; Kawahara, T.; Matsuura, Y.; Nishikawa, Y. *EMBO J.* **1990**, *9*, 4259–4265.